A Computational Method for High-Frequency Oleodynamics, Application to Hydraulic-Shock-Absorber Designs

B. Koren [1], P.F.M. Michielsen [2], J.W. Kars [3] and P. Wesseling [4]

Abstract. To predict high-frequency oil-flow phenomena in hydraulic-shock-absorber designs, a mathematical-physical model is proposed. The model consists of the 2-D unsteady Euler equations in axial-symmetric coordinates and an appropriate equation of state for oil. The main topic of the paper is the development of a numerical method for these equations. A new Osher-type flux-difference splitting scheme is derived for it. The mathematical-physical model and its numerical approximation are applied to a simplified part from a shock-absorber design. The method is promising as far as more realistic computations are concerned.

1 INTRODUCTION

1.1 Problem definition

Hydraulic shock absorbers find their main application in vehicles (trains, cars, motor-cycles, ...). A major challenge in designing new hydraulic shock absorbers is to predict and prevent unwanted high-frequency phenomena in the interior oil flow. For that purpose, the availability of a state-of-the-art computational method for hydro- (i.e. oleo-) dynamics would be helpful. At the KONI company, a start has been made in developing and applying such a method. The method is described in the present paper.

After a brief outline of construction and principles of a typical shock-absorber design (Section 1.2), in Section 2 its geometry and oleodynamics are modelled. In Section 3 the numerical method is presented: first the space discretization method for the system of equations that describe the oil flow (Section 3.1) and next the time-integration method (Section 3.2). The space discretization is partly new (a novel flux-difference splitting scheme for inviscid, compressible oil flow is presented). The time integration is standard (classical fourth-order accurate, four-stage Runge-Kutta). The paper ends with numerical results (Section 4) and concluding remarks (Section 5).

1.2 Brief outline of a shock-absorber design

For the typical shock-absorber design depicted in Figure 1, a quick impression is given of the relevant construction parts and working principles.

The major parts of the shock absorber are a cylinder (3 in Figure 1) filled with oil (plus a small fraction of gas), and with a piston with rod in it (4 and 1 in Figure 1). The piston rod can move through a bearing, the guide (2 in Figure 1). With its lower pin the shock absorber can be mounted to e.g. a train bogie, in which case the piston rod can be mounted to e.g. the passenger cabin. The piston will be set into motion by an external axial force experienced by the vehicle. To this force, a good shock absorber reacts with an (almost) equally large and (almost) equally synchronous counter-force exerted by the oil. During an inward piston-stroke (compression stroke), the oil flows through orifices in the piston from the lower piston-clearance (the compression volume, CV in Figure 1) into the upper piston-clearance (the rebound volume, RV in Figure 1). The piston orifices are normally shut off by a valve (the check valve, B in Figure 1). To compensate for volume occupied by the piston rod during a compression stroke, oil flows through orifices in the guide, into the reservoir (R in Figure 1) in between the cylinder with piston and a secondary outer cylinder. The orifices in the guide are usually shut off as well (by the so-called damping valves, A in Figure 1). From the reservoir the oil can flow into the compression volume. During the compression stroke this will not occur, since then the pressure in the compression volume is higher than in the reservoir. But during the following outward piston stroke the pressure in the compression volume becomes lower than in the reservoir and oil will flow from the reservoir through the foot valve (C and 5 in Figure 1), back into the compression volume. The points and durations of time of the various valve movements play an important role in the proper working of

[1] CWI, P.O. Box 94079, 1090 GB Amsterdam, The Netherlands
[2] KONI B.V., P.O. Box 1014, 3260 AA Oud-Beijerland, The Netherlands
[3] KONI B.V., P.O. Box 1014, 3260 AA Oud-Beijerland, The Netherlands
[4] Delft University of Technology, P.O. Box 5031, 2600 GA Delft, The Netherlands

Computational Fluid Dynamics '96
Published in 1996 by John Wiley & Sons Ltd.

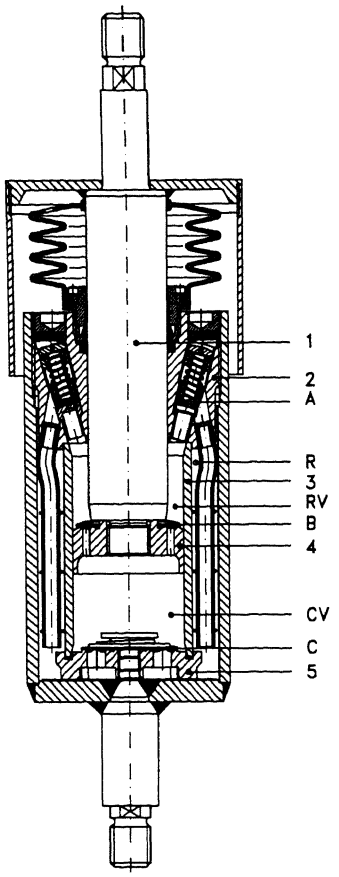

Figure 1. Cross-section of a shock-absorber design (© KONI): 1. piston rod, 2. guide, 3. inner cylinder, 4. piston, 5. foot assembly, A. damping valve, B. check valve, C. foot valve, CV. compression volume, RV. rebound volume, R. reservoir.

the shock absorber. This holds in particular for the damping valves.

Concerning unwanted high-frequency oil-flow phenomena (reaction forces) that may be generated in a shock absorber, we hypothesize that these are mainly related to pressure waves travelling to and fro in the rebound volume. The waves are supposed to reflect at closed damping and check valves. During reflection of the waves, the damping valves may quickly open (and close), violating design principles. These spurious movements of the damping valves may cause high-frequency pressure perturbations that may be transmitted directly (through construction parts) to the passenger cabin. In the next section we propose a mathematical-physical model for oil flow in the rebound volume. The model allows a first investigation of the pressure-wave hypothesis.

2 OIL-FLOW MODELLING IN REBOUND VOLUME

2.1 Geometry

The rebound volume, as depicted in Figure 1, is almost axially symmetric. For simplicity, we approximate it as axial-symmetric. Further we take the damping valve closed and the check valve opened. A sketch is given in Figure 2a. A difficulty of the geometry in Figure 2a in case of inviscid fluid-flow computations is that no unique solution exists for it; in its backward-facing-step regions, vortices of arbitrary strength are allowed. To ensure uniqueness in the inviscid case, we remove all steps, see Figure 2b.

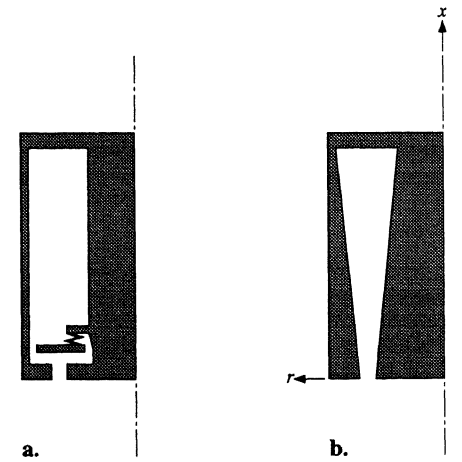

Figure 2. Schematized rebound volumes. **a.** Axial-symmetric, with damping valve closed and check valve opened. **b.** Without forward and backward facing steps.

2.2 Oil-flow equations

To investigate the effects of propagating pressure waves, an inviscid model suffices. To include nonlinear effects (shocks) and to facilitate future extensions of the flow model, as governing equations we take the Euler equations, in axial-symmetric coordinates (Figure 2b) given by:

$$\frac{\partial q}{\partial t} + \frac{\partial f(q)}{\partial x} + \frac{\partial g(q)}{\partial r} = -\frac{1}{r} S(q), \tag{1}$$

$$q = \begin{pmatrix} \rho \\ \rho u \\ \rho v \end{pmatrix}, \tag{2}$$

$$f(q) = \begin{pmatrix} \rho u \\ \rho u^2 + p \\ \rho uv \end{pmatrix}, \quad g(q) = \begin{pmatrix} \rho v \\ \rho vu \\ \rho v^2 + p \end{pmatrix}, \tag{3}$$

$$S(q) = \begin{pmatrix} \rho v \\ \rho vu \\ \rho v^2 \end{pmatrix}. \tag{4}$$

Here u and v denote the velocity components in axial (x-) and radial (r-) direction, respectively, and ρ denotes the density and p the pressure.

The system is completed by the equation of state, for which we take

$$p - p_0 = K\left(\frac{\rho}{\rho_0} - 1\right), \tag{5}$$

with K a fluid constant, and p_0 and ρ_0 the reference pressure and density, respectively. In fact (5) is a linearized version of Tait's equation of state [10]. The equation of state (5) implies isentropy. Hence, it may be substituted into the general definition of the speed of sound: $c \equiv \sqrt{\left(\frac{dp}{d\rho}\right)_s}$, yielding

$$c = c_0 \equiv \sqrt{\frac{K}{\rho_0}}. \tag{6}$$

2.3 Boundary and initial conditions

System (1) – (5) is hyperbolic with respect to time. Therefore the number of conditions to be imposed at a boundary should equal the number of characteristics entering the domain at that boundary. Two types of boundaries occur in the rebound volume's geometry as depicted in Figure 2b: (i) solid impermeable wall and (ii) subsonic inflow. Interpreting a solid impermeable wall as the limit of subsonic outflow, the number of boundary conditions to be imposed there should equal one. (As is standard, a zero normal velocity component will be imposed.) Across a subsonic inflow boundary, for the present system of three equations, two characteristics enter the domain, which implies that the number of boundary conditions to be imposed there should be two. In the present case, by these two subsonic inflow conditions the opening and closing of the check valve should be modelled. We refrain from introducing a complete model of the valve's dynamics. Only the check valve's kinematics is modelled and merely implicitly, viz. by specifying the velocity component normal to the boundary as a function of time: $u(x = 0,r,t) = u_{in}(t)$, given in Figure 3.

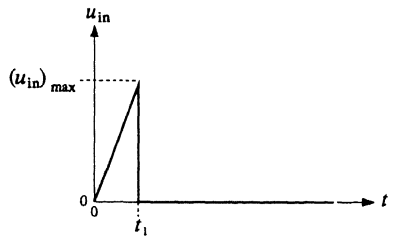

Figure 3. Sawtooth-type inflow velocity.

The valve's closing is simply taken as a discontinuity in time: at $t = t_1$, u_{in} drops instantaneously from $(u_{in})_{max}$ to zero. The values of $(u_{in})_{max}$ and t_1 can be varied by the user. As the second condition at the inflow boundary, we simply impose a zero tangential velocity component: $v(x = 0,r,t) = 0$, $t \geq 0$.

All boundary conditions imposed concern the oil's kinematics only; pressure (or density) is not imposed at any boundary. The pressure is put on a proper value through the initial conditions. As the initial solution we take the hydrostatic one: $u(x,r,t = 0) = v(x,r,t = 0) = 0$ and $p(x,r,t = 0) = p_0$, where p_0 can be chosen by the user.

3 NUMERICAL METHOD

To allow for discontinuous solutions, following Lax [4], equation (1) is rewritten in the integral form

$$\iint_{\Omega^*} \frac{\partial q}{\partial t} dx dr + \oint_{\partial\Omega^*} \left(f(q)\cos\phi + g(q)\sin\phi\right) ds = \iint_{\Omega^*} -\frac{1}{r}S(q) dx dr, \tag{7}$$

where Ω^* is an arbitrary subdomain of the computational domain Ω, $\partial\Omega^*$ the boundary of Ω^*, and $\cos\phi$ and $\sin\phi$ the x- and r-components of the outward unit normal on $\partial\Omega^*$. For the present low-subsonic oil-flow computations, use of the integral form is not as mandatory as in e.g. supersonic gasdynamics. However, no reasons exist for not applying it. In the discretization of (7) we follow the method-of-lines approach, so the spatial discretization and the temporal integration are considered separately.

3.1 Space discretization

A straightforward space discretization is obtained by subdividing Ω into quadrilateral, cell-centred finite volumes. Per finite volume we need to evaluate the net flux of mass and momentum across each cell face, and the source term integrated over the cell.

3.1.1 Flux evaluation

For the present problem, a numerical flux function needs to be chosen which accurately models the propagation of pressure waves. In our opinion, for this purpose upwind schemes are better suited than central schemes. As type of upwind scheme, we prefer a 1-D flux-difference splitting one. As shown in [6], flux-difference splitting schemes render well-resolved shear layers (particularly contact discontinuities). As specific flux-difference splitting scheme, we prefer the Osher-type [8] since it directly gives a physically proper boundary-condition treatment. For the present set of equations, (1) – (5), the corresponding Osher-type scheme does not yet exist. It will be constructed hereafter.

An Osher-type scheme for 2-D isentropic Eulerian oil flow
In Osher-type schemes, the numerical flux function $F(q_l,q_r)$ is defined as

$$F(q_l,q_r) = f(q_l) + \int_{q_l}^{q_r} \frac{df(q)}{dq}^{-} dq =$$

$$f(q_r) - \int_{q_l}^{q_r} \frac{df(q)}{dq}^{+} dq =$$

$$1/2\,(f(q_l) + f(q_r)) - 1/2 \int_{q_l}^{q_r} \left| \frac{df(q)}{dq} \right| dq, \qquad (8)$$

where $\frac{df(q)}{dq}^{-}$ is the negative eigenvalue part of $\frac{df(q)}{dq}$, $\frac{df(q)}{dq}^{+}$ the positive eigenvalue part, and where $\left| \frac{df(q)}{dq} \right| \equiv \frac{df(q)}{dq}^{+} - \frac{df(q)}{dq}^{-}$. Osher has proposed integration paths in state space (for the integrals in (8)) that make the integration trivial. For theoretical background and an impression how an Osher-type scheme is constructed, see [8]. (There the construction is done for the hyperbolic systems that describe 1-D non-isentropic Lagrangian gas flow, 1-D non-isentropic Eulerian gas flow and 2-D isentropic Eulerian gas flow.) To construct an Osher-type scheme for the present 2-D Eulerian oil flow described by (1) – (5), only the homogeneous quasi-linear form

$$\frac{\partial q}{\partial t} + \frac{df(q)}{dq}\frac{\partial q}{\partial x} = 0 \qquad (9)$$

needs to be considered. With q according to (2), $f(q)$ according to (3), $p(\rho)$ according to (5), and the speed of sound c_0 according to (6), for the Jacobian $\frac{df(q)}{dq}$ it follows then

$$\frac{df(q)}{dq} = \begin{pmatrix} 0 & 1 & 0 \\ -u^2 + c_0^2 & 2u & 0 \\ -uv & v & u \end{pmatrix}. \qquad (10)$$

The eigenvalues of the Jacobian are

$$\lambda_1 = u - c_0, \quad \lambda_2 = u, \quad \lambda_3 = u + c_0. \qquad (11)$$

The fact that the eigenvalues vary with u only (since c_0 is constant) means that steepening of solution gradients (i.e. the nonlinearity) comes from u only. The eigenvectors corresponding with the above eigenvalues are

$$R_1 = \begin{pmatrix} \frac{1}{v} \\ \frac{u-c_0}{v} \\ 1 \end{pmatrix}, \quad R_2 = \begin{pmatrix} 0 \\ 0 \\ 1 \end{pmatrix}, \quad R_3 = \begin{pmatrix} \frac{1}{v} \\ \frac{u+c_0}{v} \\ 1 \end{pmatrix}. \qquad (12)$$

The eigenvectors are linearly independent. Referring to the theory in [8], R_2 is linearly degenerate, and R_1 and R_3 are genuinely nonlinear. Hence, R_1 and R_3 should correspond with simple waves (compression or expansion waves), and R_2 with a contact discontinuity. We consider now the integration path in state space. Osher has proposed to take a path built up of subcurves, where each subcurve is tangential (in state space) to one of the eigenvectors. With the present three eigenvectors, according to Osher the integration path is as depicted in Figure 4a. In this path the ordering of eigenvectors, when going from q_l to q_r is R_3,R_2,R_1. The reverse (R_1,R_2,R_3 in going from q_l to q_r) is also possible (Figure 4b). The idea of reversion stems from Hemker & Spekreijse [1], who (for the 2-D non-isentropic perfect-gas Euler equations) named the ordering

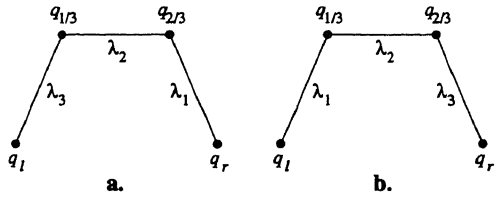

Figure 4. Two variants of Osher-path in state space. **a.** O-variant. **b.** P-variant.

proposed by Osher the O(riginal)-variant and their own the P(hysical)-variant.

The advantage of the P-variant over the O-variant is its better computational efficiency, particularly for subsonic flow computations. This can be explained as follows. With the integration path tangential to the eigenvectors, the integral evaluation boils down to ordinary flux evaluations at a few points along the integration path. Because two of the three eigenvalues are nonlinear, and one linearly degenerate, this number of points is five at a maximum. For the fully subsonic flows to be considered here, with the P-variant it is only one (!): $F(q_l,q_r) = f(q_{l/3})$. (With the O-variant this would be three: $F(q_l,q_r) = f(q_l) - f(q_{2/3}) + f(q_r)$.) Given the fact that the present computations are fully subsonic, here one can take full advantage of the P-variant.

To evaluate Osher's numerical flux function, the intersection states $q_{1/3}$ and $q_{2/3}$ need to be known. They follow from the Riemann invariants ψ_l^k, $k = 1,2,3$, $l = 1,2,3$, $l \neq k$ valid along the subcurves. The Riemann invariants satisfy

$$\nabla\psi_l^k \cdot R_k = 0, \quad k = 1,2,3, \quad l = 1,2,3, \quad l \neq k, \qquad (13)$$

$$\nabla \equiv \left(\frac{\partial}{\partial q_1}, \frac{\partial}{\partial q_2}, \frac{\partial}{\partial q_3} \right). \qquad (14)$$

Hence, ψ_l^2, $l = 1,3$ simply have to satisfy

$$\frac{\partial \psi_l^2}{\partial q_3} = 0, \quad l = 1,3. \qquad (15)$$

These Riemann invariants follow directly, in conservative variables: $\psi_1^2 = q_1$, $\psi_3^2 = q_2$, or in primitive variables: $\psi_1^2 = \rho$, $\psi_3^2 = u$. (In case of a linearly degenerate eigenvalue one of the Riemann invariants is identical to that eigenvalue.) The Riemann invariants ψ_l^1, $l = 2,3$ along the first subcurve have to satisfy

$$q_1 \frac{\partial \psi_l^1}{\partial q_1} + (q_2 - c_0 q_1)\frac{\partial \psi_l^1}{\partial q_2} + q_3 \frac{\partial \psi_l^1}{\partial q_3} = 0, \quad l = 2,3. \qquad (16)$$

The partial differential equation for the Riemann invariants along the third subcurve is almost identical to (16); it only differs in a sign in the second coefficient. (As a consequence, one of the corresponding Riemann invariants ψ_l^3, $l = 1,2$ will probably also have a difference with ψ_l^1, $l = 2,3$ in a single sign only.) Given the fact that both primitive variables ρ and u are constant along the second subcurve, they are no candidates for being a Riemann invariant along the first and

third subcurve. The remaining primitive variable v *is*; substitution of $\psi_2^l = \frac{q_2}{q_l}$ into (16) learns that it is a Riemann invariant indeed. So far, there is a good resemblance with the 2-D Eulerian gas case from [8]. Expecting a further resemblance, for the remaining Riemann invariant along the first subcurve we try $\psi_3^l = u + Q(\rho) = \frac{q_2}{q_l} + Q(q_l)$. Substitution into (16) yields the simple ordinary differential equation $\frac{dQ}{dq_l} = \frac{c_0}{q_l}$. Integration yields $Q = c_0(\ln\rho + C)$, with C an integration constant. We take $C = -\ln\rho_0$, leading to the Riemann invariant $\psi_3^l = u + c_0 \ln\left(\frac{\rho}{\rho_0}\right)$. It can be directly seen that along the third subcurve the Riemann invariants are: $\psi_1^3 = v$, $\psi_2^3 = u - c_0 \ln\left(\frac{\rho}{\rho_0}\right)$. The resulting Osher path is summarized in Figure 5.

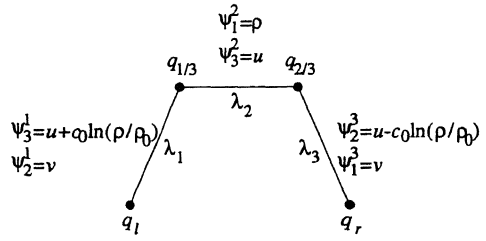

Figure 5. P-variant Osher-path for 2-D isentropic Eulerian oil flow.

For the intersection states $q_{1/3}$ and $q_{2/3}$ it follows:

$$\begin{pmatrix} \rho_{1/3} \\ u_{1/3} \\ v_{1/3} \end{pmatrix} = \begin{pmatrix} \rho_{1/2} \\ u_{1/2} \\ v_l \end{pmatrix}, \quad \begin{pmatrix} \rho_{2/3} \\ u_{2/3} \\ v_{2/3} \end{pmatrix} = \begin{pmatrix} \rho_{1/2} \\ u_{1/2} \\ v_r \end{pmatrix}, \tag{17}$$

where

$$\rho_{1/2} \equiv \sqrt{\rho_l \rho_r e^{\frac{u_l - u_r}{c_0}}}, \tag{18}$$

$$u_{1/2} \equiv 1/2(u_l + u_r) + 1/2c_0 \ln\left(\frac{\rho_l}{\rho_r}\right). \tag{19}$$

This concludes the construction of the present Osher scheme for given left and right cell-face states.

The Osher-type boundary-condition treatment for 2-D isentropic Eulerian oil flow If the cell face coincides with the boundary of the computational domain, in case of a left or right boundary, q_l or q_r, respectively, does not exist; it is outside the computational domain. Just *at* the boundary is the state q_b. This boundary state q_b can be determined by ingoing and outgoing characteristic information (i.e. by proper boundary conditions and Riemann invariants, respectively). An upwind treatment of boundary conditions fits well in Osher-type schemes. The theoretical basis for Osher's handling of boundary conditions is given in [7]. Following the same approach as in the foregoing section, here we will also mainly restrict ourselves to reinterpreting this theory in terms of the Osher-path. The reinterpretation will be done for the types of boundaries that we have to deal with here: subsonic inflow and solid impermeable wall.

Subsonic inflow In the present application we only have to deal with the case of a subsonic inflow boundary at the left (Figure 6a). For completeness, the case with boundary at the right (Figure 6b) is also considered.

Figure 6. The two cases of subsonic inflow boundary. **a.** Boundary at the left ($0 < u_r < c_r$). **b.** Boundary at the right ($-c_l < u_l < 0$).

In both cases the Osher-path is reduced in the sense that one subcurve disappears (Figures 7a,b). The vanished subcurve corresponds with the outgoing characteristic.

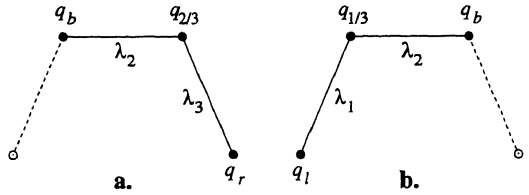

Figure 7. Reduced Osher-paths (P-variant) for subsonic inflow boundary. **a.** Boundary at the left ($0 < u_r < c_r$). **b.** Boundary at the right ($-c_l < u_l < 0$).

In both cases two of the three components of q_b should be given by boundary conditions. In Section 2.3 it has been decided to impose u_b and v_b. The remaining unknown component of q_b can be determined, together with the unknown state $q_{2/3}$ (left boundary) or $q_{1/3}$ (right boundary), by using the corresponding Riemann invariants ($\psi_1^2, \psi_3^2, \psi_1^3, \psi_2^3$ for the left-boundary case and $\psi_2^1, \psi_3^1, \psi_1^2, \psi_3^2$ for the right). For the left-boundary case we find

$$\begin{pmatrix} \rho_b \\ u_b \\ v_b \end{pmatrix} = \begin{pmatrix} \rho_{1/2} \\ u_{\text{in}}(t) \\ 0 \end{pmatrix}, \quad \begin{pmatrix} \rho_{2/3} \\ u_{2/3} \\ v_{2/3} \end{pmatrix} = \begin{pmatrix} \rho_{1/2} \\ u_{\text{in}}(t) \\ v_r \end{pmatrix}, \tag{20}$$

$$\rho_{1/2} = \rho_r e^{\frac{u_{\text{in}}(t) - u_r}{c_0}}, \tag{21}$$

and for the right (which is not in the present shock-absorber model):

$$\begin{pmatrix} \rho_{1/3} \\ u_{1/3} \\ v_{1/3} \end{pmatrix} = \begin{pmatrix} \rho_{1/2} \\ u_{\text{in}} \\ v_l \end{pmatrix}, \quad \begin{pmatrix} \rho_b \\ u_b \\ v_b \end{pmatrix} = \begin{pmatrix} \rho_{1/2} \\ u_{\text{in}} \\ v_{\text{in}} \end{pmatrix}, \tag{22}$$

$$\rho_{1/2} = \rho_l e^{\frac{u_l - u_{\text{in}}}{c_0}}. \tag{23}$$

Solid impermeable wall In the present rebound-volume model both a left and a right wall (Figures 8a,b) occur.

Figure 8. The two cases of solid impermeable wall boundary. **a.** Boundary at the left. **b.** Boundary at the right.

As mentioned in Section 2.3 only one component of q_b is prescribed by a boundary condition. The remaining two components are determined from the two Riemann invariants in the reduced Osher-path: ψ_1^3 and ψ_2^3 in the left-boundary case (Figure 9a), and ψ_2^1 and ψ_3^1 in the right-boundary case (Figure 9b). For the left-boundary case we find

$$\begin{pmatrix} \rho_b \\ u_b \\ v_b \end{pmatrix} = \begin{pmatrix} \rho_r e^{\frac{-u_r}{c_0}} \\ 0 \\ v_r \end{pmatrix}, \tag{24}$$

and for the right-boundary case

$$\begin{pmatrix} \rho_b \\ u_b \\ v_b \end{pmatrix} = \begin{pmatrix} \rho_l e^{\frac{u_l}{c_0}} \\ 0 \\ v_l \end{pmatrix}. \tag{25}$$

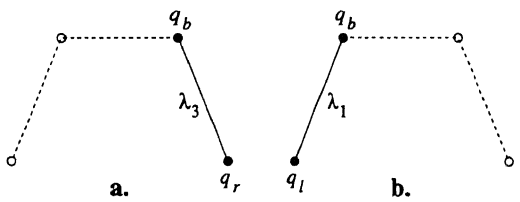

Figure 9. Reduced Osher-paths (P-variant) for solid impermeable wall boundary. **a.** Boundary at the left. **b.** Boundary at the right.

This completes the boundary-condition treatment necessary for our application. Other types (subsonic outflow with pressure or outflow velocity specified, supersonic in- or outflow, ...) can be quickly constructed.

The interpolation for the left and right cell-face states Besides for the numerical flux function $F(q_l,q_r)$, a choice also needs to be made for its two arguments q_l and q_r. Both cell-face states are determined by higher-order accurate state interpolation. (The interpolation is done in a 1-D fashion, which is consistent with the application of a 1-D flux-difference splitting scheme.) To avoid spurious non-monotonicity, a limiter function is applied, viz. the one from [3], in the notations of Sweby [9]:

$$\phi(r) = \max(0, \min(2r, \min(1/3 + 2/3r, 2))). \tag{26}$$

This limiter is such that inside Sweby's monotonicity domain it coincides to the maximum extent with the for accuracy reasons favourable $\kappa = 1/3$-scheme, see [5].

3.1.2 *Source-term evaluation*

The way of evaluating the source-term integral occurring in (7) is straightforward. $S(q)$ is taken piecewise constant over each finite volume $\Omega_{i,j}$, which directly leads to

$$\int\int_{\Omega_{i,j}} -\frac{1}{r} S(q) \mathrm{d}x\mathrm{d}r = -\frac{1}{r_{i,j}} S(q_{i,j}) A_{i,j}, \tag{27}$$

where $A_{i,j}$ is the area of finite volume $\Omega_{i,j}$.

3.2 Time integration

For the time discretization of the semi-discrete equation

$$\int\int_{\Omega_{i,j}} \frac{\partial q}{\partial t} \mathrm{d}x\mathrm{d}r = R_{i,j}(\ldots, q_{i,j}, \ldots), \tag{28}$$

where $R_{i,j}(\ldots, q_{i,j}, \ldots)$ denotes the total space-discretization contribution in finite volume $\Omega_{i,j}$ (consisting of both the discrete flux and source-term contributions just discussed), we take the standard explicit four-stage Runge-Kutta scheme.

Formally, the time step is subjected to restrictions imposed by accuracy, stability and monotonicity. For a short overview of theory on monotonicity bounds for the time step, see [2]. The stability bound imposed on the time step is the CFL-condition. The accuracy bound on the time step is determined by the requirement that the sawtooth inlet velocity profile (Figure 3), particularly the jump at $t = t_1$, is imposed sufficiently accurate. Of all three bounds, the one for accuracy is the most severe.

4 NUMERICAL RESULTS

Here a quick impression is given of the performances of the mathematical-physical model and the numerical method. The results have been obtained for the geometry given in Figure 2b, and for $p_0 = 1$ bar and $\rho_0 = 870$ kg/m^3.

In Figures 10 and 11 the beginning of a pressure history is depicted as computed along the piston rod and at the middle of the rebound volume's upper boundary, respectively. The first pressure wave given in both figures is directly caused by the check valve's opening. The second pressure wave is the reflection of the first wave. The graph shows the start of the travelling to and fro of pressure waves in the rebound volume. The negative pressures that are found are not believed to be a numerical artefact, but – instead – an illustration of the still existing shortcomings of the physical model, such as the zero diffusion and the lack of a cavitation model.

A noticeable fact is that the pressure variations are large; unwanted opening of the damping valves may easily be the result.

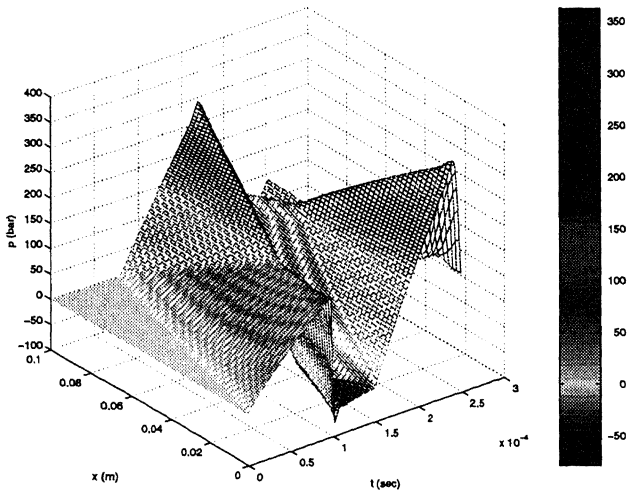

Figure 10. Beginning of pressure history along the piston rod.

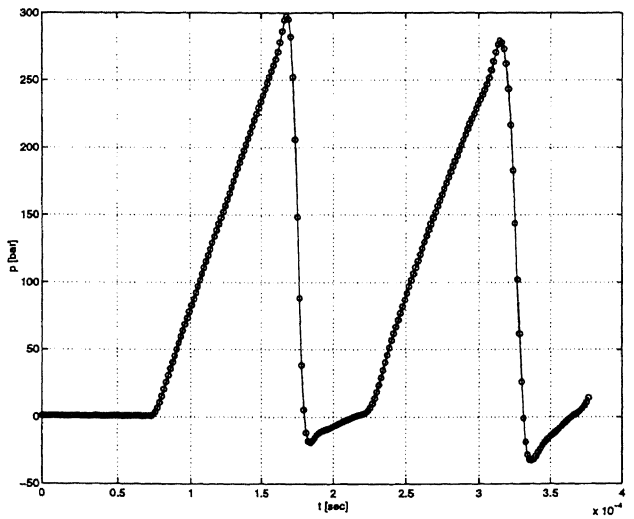

Figure 11. Beginning of pressure history in the middle of the rebound volume's upper boundary.

5 CONCLUSIONS

From the viewpoint of shock-absorber design, many conclusions can be drawn, but here we restrict ourselves to the observation that the predicted pressure variations are large and may easily cause spurious opening and closing of valves.

Our ideas for future work are: (i) to take the geometry closer to that given in Figure 1, (ii) to use an equation of state which takes into account multiphase behaviour, (iii) to introduce a cavitation model, and (iv) to extend the present Euler equations with viscous terms.

REFERENCES

[1] P.W. Hemker and S.P. Spekreijse, 'Multiple grid and Osher's scheme for the efficient solution of the steady Euler equations', *Applied Numerical Mathematics*, **2**, 475–493, (1986).

[2] W. Hundsdorfer, B. Koren, M. van Loon, and J.G. Verwer, 'A positive finite-difference advection scheme', *Journal of Computational Physics*, **117**, 35–46, (1995).

[3] B. Koren, *A robust upwind discretization method for advection, diffusion and source terms*, volume 45 of *Notes on Numerical Fluid Mechanics*, 117–138, Vieweg, Braunschweig, 1993.

[4] P.D. Lax, 'Hyperbolic systems of conservation laws II', *Communications on Pure and Applied Mathematics*, **10**, 537–566, (1957).

[5] B. van Leer, *Upwind-difference methods for aerodynamic problems governed by the Euler equations*, volume 22 of *Lectures in Applied Mathematics*, 327–336, American Mathematical Society, Providence, RI, 1985.

[6] B. van Leer, J.L. Thomas, P.L. Roe, and R.W. Newsome. A comparison of numerical flux formulas for the Euler and Navier-Stokes equations. AIAA paper 87-1104.

[7] S. Osher and S. Chakravarthy, 'Upwind schemes and boundary conditions with applications to Euler equations in general geometries', *Journal of Computational Physics*, **50**, 447–481, (1983).

[8] S. Osher and F. Solomon, 'Upwind difference schemes for hyperbolic systems of conservation laws', *Mathematics of Computation*, **38**, 339–374, (1982).

[9] P.K. Sweby, 'High resolution schemes using flux limiters for hyperbolic conservation laws', *SIAM Journal on Numerical Analysis*, **21**, 995–1011, (1984).

[10] P.A. Thompson, *Compressible-Fluid Dynamics*, McGraw-Hill, New York, 1972.